Journal of Hydrology (2007) 337, 269–283



available at www.sciencedirect.com

ScienceDirect

journal homepage: www.elsevier.com/locate/jhydrol



# Evapotranspiration over a Japanese cypress forest. I. Eddy covariance fluxes and surface conductance characteristics for 3 years

**Yoshiko Kosugi [a,*], Satoru Takanashi [a], Hiroki Tanaka [a,b], Shinjiro Ohkubo [a], Makoto Tani [a], Masato Yano [a,d], Tatsuya Katayama [a,c]**

[a] *Laboratory of Forest Hydrology, Division of Environmental Science and Technology, Graduate School of Agriculture, Kyoto University, Kyoto 606-8502, Japan*
[b] *Graduate School of Environmental Studies, Nagoya University, 464-8601, Japan*
[c] *NTT Communications Co., Tokyo, Japan*
[d] *UFJ Institute Ltd., 1-11-7, Shimbashi, Minato-Ku, Tokyo 105-8631, Japan*

Received 30 November 2006; received in revised form 26 January 2007; accepted 26 January 2007

**KEYWORDS**
Evapotranspiration;
Coniferous forest;
Eddy covariance;
Energy budget;
Surface conductance

**Summary** Evapotranspiration above a Japanese cypress (*Chamaecyparis obtusa* Sieb. et Zucc.) forest with complex topography in central Japan were observed for 3 years using the eddy covariance method. The observations describe the magnitude and seasonal and inter-annual variations in sensible and latent heat fluxes, evapotranspiration and the parameters describing bulk canopy characteristics. Average annual evapotranspiration over the period was approximately 735 mm. Despite large fluctuations in precipitation (1179–1971 mm) during the 3 years, inter-annual fluctuations in evapotranspiration were small. Midday average dry canopy surface conductance was 6.7 mm $s^{-1}$ during midseason and decreased in winter. The midday average dry canopy decoupling factor ($\Omega$) was 0.21 during midseason and decreased in winter. This forest is characterized by relatively small values of surface conductance and decoupling factor compared to other forests. However, several other coniferous forests show smaller values. Surface conductance, and thus stomatal regulation, is important in controlling dry-canopy transpiration in this forest. Inter-annual fluctuations of bulk parameters were small; surface conductance characteristics affected by soil moisture did not vary between dry and wet years.
© 2007 Elsevier B.V. All rights reserved.

* Corresponding author. Tel.: +81 75 753 6089; fax: +81 75 753 6088.
*E-mail address:* ykosugi@kais.kyoto-u.ac.jp (Y. Kosugi).

0022-1694/$ - see front matter © 2007 Elsevier B.V. All rights reserved.
doi:10.1016/j.jhydrol.2007.01.039

## Introduction

Typical plantation forests in the mountains of Japan are evergreen coniferous forests. Evapotranspiration from these forests greatly influences hydrological and micrometeorological processes and also the environmental functions of the forests. Evaluation of evapotranspiration using eddy covariance heat fluxes coupled with micrometeorological data allows analysis of the factors that control evapotranspiration. Analysis of dry-canopy transpiration measured with the eddy covariance method will yield information on stomatal behavior and influence on heat, water vapor, and carbon dioxide fluxes. Understanding how dry canopy transpiration interacts with photosynthesis and is influenced by stomatal regulation is critical for understanding gas-exchange processes. Diurnal, seasonal, and interannual fluctuations in evapotranspiration and bulk parameters, which include surface conductance (Monteith, 1973) and decoupling factor (McNaughton and Jarvis, 1983), can and should be evaluated for various vegetation types.

Results from the eddy covariance method have shown small values of surface conductance in coniferous forests. For example, Baldocchi et al. (1997) reported daytime (6:00—19:00) average values of 2 mm $s^{-1}$ for a boreal jack pine forest. Kelliher et al. (1998) found daily mean values between 0.5 and 2.5 mm $s^{-1}$ in a pine forest in central Siberia. Values depended on soil water content and had a maximum of 7 mm $s^{-1}$. Kelliher et al. (1997) found a maximum value of 10 mm $s^{-1}$ for a larch forest in eastern Siberian. Humphreys et al. (2003) calculated midday (10:00—15:00) average surface conductance of 4.2 and 2.9 mm $s^{-1}$ in a Douglas-fir forest for three fair summer days in wet and dry years, respectively. The average midday dry canopy decoupling factor in summer in the same forest was 0.24. Small values in coniferous stands relate more to stand type than to climatic region. Average surface conductance in a boreal aspen forest averaged 8.4 mm $s^{-1}$ and peaked at 30 mm $s^{-1}$ during the day (Blanken et al., 1997) when the photosynthetic photon flux density (PPFD) exceeded 200 μmol $m^{-2}$ $s^{-1}$. Midseason average daytime values weighted by net radiation were approximately 10 mm $s^{-1}$ for a North American temperate deciduous forest (Wilson and Baldocchi, 2000). In addition, this same forest was characterized by a large decoupling factor (0.41) for a dry midseason canopy (Wilson and Baldocchi, 2000), corresponding to large surface conductance. Tropical evergreen broadleaved forests also showed larger values of surface conductance as reviewed by Roberts et al. (2005). Amazonian rainforests have the values from 10 to 25 mm $s^{-1}$ with an early-morning maximum (Grace et al., 1995). Maximum values computed for two tropical evergreen broadleaved forests in Malaysia using the Bowen ratio method were 35 mm $s^{-1}$ (Tani et al., 2003). Daily mean values computed using the eddy covariance method were 16 mm $s^{-1}$ during a wet period (Kumagai et al., 2004).

The small surface conductance and decoupling factor computed using eddy covariance data for several coniferous stands may not be typical for all coniferous stands. As Kelliher et al. (1995) described maximum surface conductance from 33 fields, and results included relatively large (compared to other vegetation types) maximum surface conductance for several coniferous stands. Komatsu (2003) used various flux observations at numerous sites and showed a negative relationship between canopy height and surface conductance for closed coniferous stands, which suggests that small surface conductance observed in tall coniferous stands is restrained by the water uptake. Although restricting factors for the stomatal conductance, including soil drought, phenology, and seasonality, must be analyzed at individual sites using long-term flux datasets to determine differences in evapotranspiration characteristics between forest types. It is also possible that surface conductance is underestimated in the eddy covariance method because of an energy closure problem (the imbalance problem), i.e., sensible and latent heat fluxes are underestimated. Accurately measuring energy fluxes for the eddy covariance method may be difficult, especially for forest sites with complex topography. The imbalance problem has been noted in many studies (e.g., Wilson et al., 2002; Turnipseed et al., 2002; Culf et al., 2004). Whether eddy covariance data provide accurate information so that heat fluxes and evapotranspiration can be evaluated is a question that must be answered for individual sites.

In this study, we analyzed sensible and latent heat fluxes from 3 years over a Japanese cypress forest with complex topography in central Japan. The eddy covariance method was used to determine fluxes over this temperate evergreen coniferous forest, yielding information on the magnitude and seasonal and interannual variations of the sensible and latent heat fluxes, evapotranspiration, and parameters representing the bulk canopy characteristics. A detailed assessment of the energy budget closure was also performed to point out the advertences to assess the evapotranspiration using eddy covariance method with closed-path and open-path systems, which has been not been emphasized as in the case of $CO_2$ exchange.

## Method

### Site

Observations were made at the Kiryu Experimental Watershed (KEW) at 34°58′ N, 136°00′ E in Shiga Prefecture, central Japan (Fig. 1). Forests of Japanese cypress once covered this area of the Tanakami Mountains, but the forests were devastated about 1200 years ago by fire and excessive logging to build Nara and Kyoto (former capitals of Japan). The mountains remained bare for centuries. Reforestation has occurred over the last 100 years to prevent soil erosion and to provide a timber source. Consequently, most of the area is now covered with plantation forests. KEW was established in 1967 to study hydrological water circulation and to determine the roles of trees and soil in the forest. It represents one of the longest continuous research programs in Japan and has one of the longest historical hydrological datasets. An experimental watershed covers 5.99 ha and ranges in elevation from 190 to 255 m (Fig. 1). Runoff rates have been observed in the watershed since 1967 (Fukushima, 1988). A meteorological observation tower is located in a small catchment within the experimental watershed; this small catchment (Matsuzawa catchment; gray zone in Fig. 1b) has an area of 0.68 ha and is covered

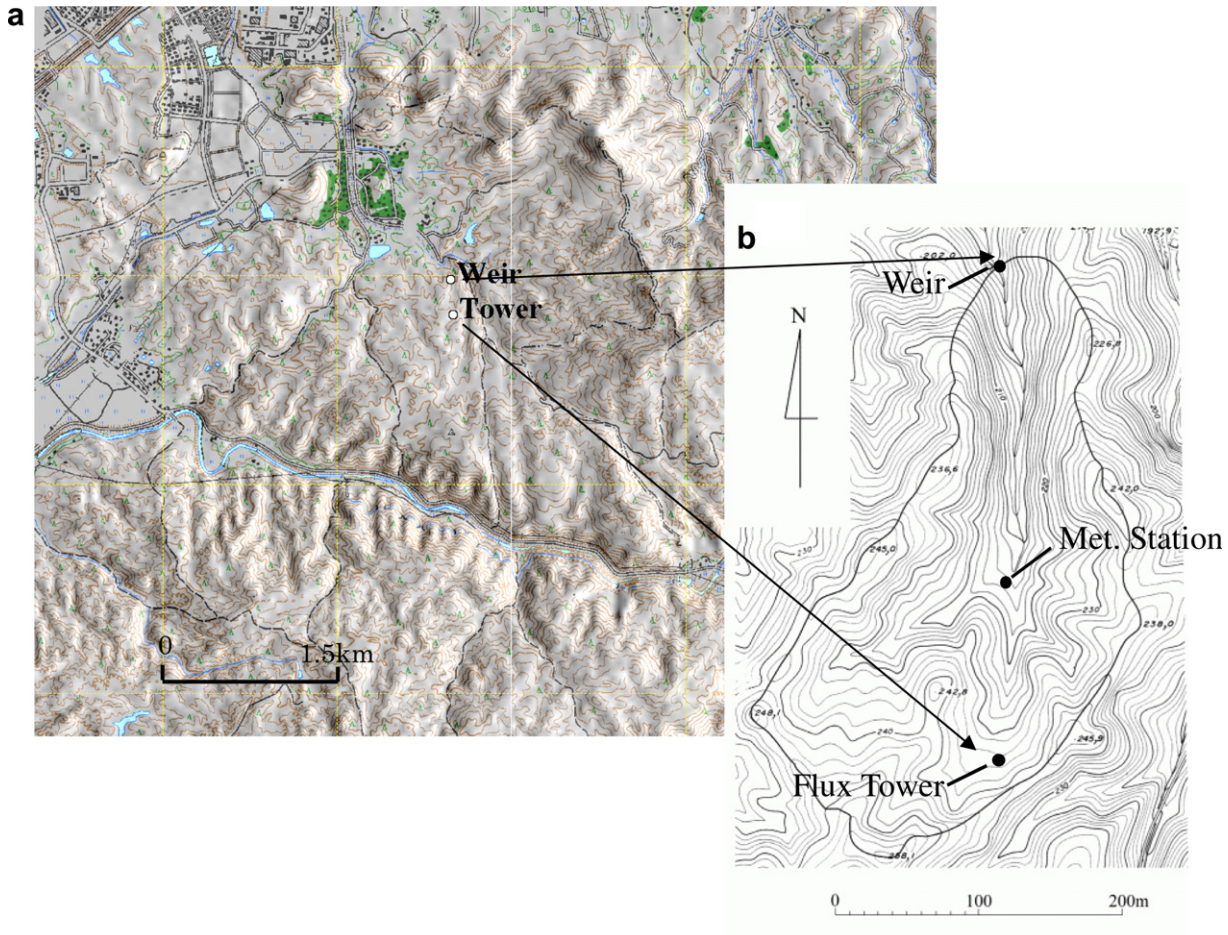



**Figure 1** Topographic map of the observation site. The gray zone denotes the small catchment where all flux and meteorological observations and ground measurements except rainfall and air temperature at open site and runoff were recorded.

mainly by *Chamaecyparis obtusa* Sieb. et Zucc. (Japanese cypress, an evergreen conifer) planted in 1959 (13.9 m average height, 21.1 m maximum height, 43 $m^{-2}$ $ha^{-1}$ basal area, and 1853 stems $ha^{-1}$ for 92% of total basal area). *Pinus densiflora* Sieb. et Zucc. and several species of deciduous broad-leaved trees are sparsely present. Pine-wilt disease in recent years has reduced *P. densiflora* stands (Hobara et al., 2001). *Eurya japonica* Thunb. dominates the forest floor. The total leaf area index (LAI), measured using a LAI-2000 plant canopy analyzer (LI-COR Inc., USA), ranges from 4.5 to 5.5 with a little seasonal fluctuation. The entire watershed is underlain by weathered granite with abundant amounts of albite. The $A_0$ horizon has a humus form with no apparent *H* horizon. Ohte et al. (1995, 1997) detailed the physical and chemical properties of the soil in the watershed. The topographic map of the area (Fig. 1b) shows a slight northward inclination of approximately 9.2°. The surrounding area is a national forest dominated by *C. obtusa*. Winds blow mainly from the north or west during the day and from the south at night (see Fig. 7 for details) with no significant seasonal differences. The forest fetch in a northwest direction is about 750 m, while the fetch in the other directions exceeds 2000 m. The model of Schuepp et al. (1990) suggests that more than 80% of the measured flux originates from within the actual forest about 92% of the time during the day and 81% of the time at night (Takanashi et al., 2005). The annual mean air temperature measured at an open screen site from 1997 to 2004 was 13.6 °C. The annual mean precipitation from 1972 to 2004 was 1645.0 mm. The site has a warm temperate climate. Rainfall occurs throughout the year, with a peak in summer, and little snow falls in winter.

## Measurement of eddy covariance fluxes

The existing meteorological observation tower, built in 1994 and extended in 1999, is located in the Matsuzawa catchment. Fluxes of momentum, sensible heat (*H*), and latent heat ($\lambda E$) were measured by eddy covariance methods at a tower height of 28.5 m. Data analyzed in this paper were recorded between 1 January 2001 and 31 December 2003. Air temperatures and three-dimensional wind speeds were measured with a three-dimensional sonic anemo-thermometer (model DAT-310 or DA-600 T [after 27 December 2001], KAIJO, Japan). Fast-response, closed-path infrared gas analyzers (IRGA; model LI-6262 or LI-7000 [after 9 August 2001], LI-COR Inc.) were used to measure water vapor

concentrations. Since 30 April 2002, $CO_2$ and $H_2O$ concentrations were also measured by an open-path IRGA (model LI-7500, LI-COR Inc.). The closed-path IRGA was mounted on the tower platform to minimize tube length. Air moved through a bev-a-line plastic tube (3-mm interior diameter, about 3.0 m long) and into the sampling cell at a rate of 1.0 or 1.5 l $min^{-1}$. A 1-μm Teflon filter (Pall Gelman Inc., Canada) placed near the gas inlet reduced contamination of the optical chamber. Agents to maintain dry and $CO_2$-free air in the reference cell line of closed-path sensors were changed every 2–3 weeks, and the filter and tube were changed periodically, depending on contamination. Two LI-6262 IRGAs were used; one was calibrated in the laboratory and replaced other on the platform every 2 weeks. The LI-7000, which was used starting on 9 August 2001, was periodically zero-calibrated, using nitrogen gas, on the tower platform. Span calibration was made when the sample cell was cleaned due to contamination by heavy rain. The LI-7000 is quite stable and features quick restoration to reference cell conditions after agent change because of the tubing system. Calibration drift in both IRGAs was mostly a zero shift of typically <10 ppm. The slope changes were rare; therefore, covariance measurements were not greatly affected. The open-path gas analyzer LI-7500 was mounted at an angle so that water drops could not sit on the sensor lens and the radiation effect would be minimized.

Analog signals from the sonic anemo-thermometer and IRGAs were sampled by a datalogger (NR1000 [through 6 February 2002], Keyence Co., Japan, CR10X [6 February 2002–11 April 2002] or CR23X [after 11 April 2002], Campbell Scientific, USA) at 10 Hz (8 Hz from 6 February to 11 April 2002) and sent to a personal computer. Raw data were transferred to the laboratory every 2–3 weeks. Fluxes of momentum, sensible heat, water vapor, and $CO_2$ were calculated with averaging times of 30 min.

In many studies, the three-dimensional coordinate rotation for the vertical wind velocity normal to the mean wind direction (Mcmillen, 1988) is applied assuming zero mean vertical wind. However, a planar fit rotation (e.g., Kondo and Sato, 1982; Kaimal and Finnigan, 1994; Mahrt et al., 1996; Lee, 1998) is more suitable if the mean vertical wind ($\bar{w}$) is non-zero. Fig. 2 shows the $u$–$w$ transform angle, assuming $\bar{w} = 0$, versus wind direction. Here $u$ and $w$ are the horizontal and vertical wind velocity, respectively. The light gray line shows the rotation using one plane. However, terrain slope at the study site means that the long-term mean vertical winds cannot be zero for every direction with this one-plane rotation. Therefore, a planer fit rotation with different wind directions (Wilczak et al., 2001) was applied using five expansion fans as shown by the dark gray line in Fig. 2.

Independent time lags for $H_2O$ and $CO_2$ were determined after each maintenance and data-collection cycle (typically every 2–3 weeks) so as to maximize the covariance between vertical wind velocities in the closed-path system. The median of the optimized time lag for each 30-min cycle was used as the constant for each period. The manufacturer's recommended correction for time lag in the LI7500 was included in the open-path system. Linear trends in air temperature, $CO_2$, and $H_2O$ were removed. Data spikes with values exceeding 3.5 standard deviations were replaced with interpolated values. Data spikes included only 1, 2, or 3 consecutive points. Data that were outside a set range (e.g., caused by analog communication errors) were replaced. If the number of spikes or out-of-range data exceeded 1% of the total data points for each element, then those 30 min of flux data were rejected for quality reasons. Data that did not meet the stationarity criteria (Foken and Wichura, 1996; Aubinet et al., 2000) were also rejected.

Webb, Pearman, Leuning (WPL) correction for the effect of air density fluctuations (Webb et al., 1980) was applied to open-path system data but not to closed-path system data. Fluctuations in $H_2O$ and $CO_2$ were sampled with the closed-path system in terms of mole fractions calculated by IRGA software, which included corrections due to water vapor fluctuations (Aubinet et al., 2000).

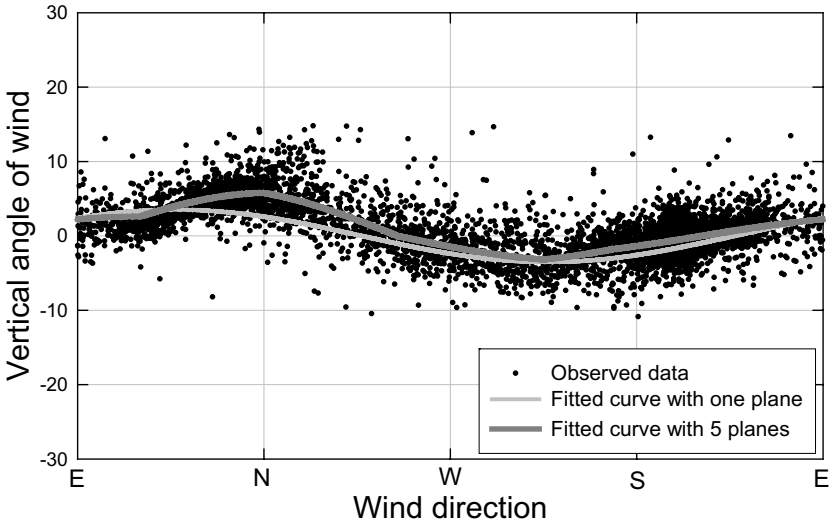



**Figure 2** Relationship between the $u$–$w$ transform angle assuming a $\bar{w} = 0$ wind direction. The light gray line shows one plane rotation. The dark gray line shows rotation using a combination of five expansion fans from the observation tower. The analysis used every 30-min dataset from 21 May to 31 October 2002.

Attenuation of density fluctuations related to the passage of air through a tube must be assessed for the closed-path system (Leuning and Moncrieff, 1990; Leuning and Judo, 1996). If co-spectral similarity is assumed between the exchange of sensible heat and latent heat, $\lambda E$ after correction is described as follows (Moore, 1986),

$$\frac{\overline{w'h'}_{cor} - \overline{w'h'}_{raw}}{\overline{w'h'}_{raw}} = \int_0^\infty \left( \frac{C_{wt}(f)}{\overline{w't'}} (1 - TF(f)) \right) df, \quad (1)$$

where $\overline{w'h'}_{cor}$ and $\overline{w'h'}_{raw}$ are covariances of $w$ and the water vapor concentration $h$ after and before correction, respectively, $C_{wt}(f)$ is the co-spectral density of $w$ and air temperature $t$, $\overline{w't'}$ is the covariance of $w$ and $t$, and TF($f$) is the net system co-spectral transfer function. The normalized co-spectra function $\frac{fC_{wt}(f)}{\overline{w't'}}$ and the transfer function TF($f$) are required to evaluate the loss ratio for latent heat flux.

Kaimal and Finnigan (1994) and Moore (1986) described a parameterization of the normalized co-spectral model for $w$ and $t$ that used Monin–Obukhov similarity theory and data from an experiment in Kansas (Kaimal et al., 1972). However, actual co-spectra at sites with complex terrain such as in our study may have significant deviations. Therefore, a parameterization based on the $w$ and $t$ data observed in this study is more suitable. The normalized co-spectra models of $w$ and $t$ are (Kaimal, 1988):

$$\begin{aligned} &\frac{nC_{wt}(n)}{\overline{w't'}} = \frac{(f(z-d)/U)}{[A + B(f(z-d)/U)]^{\frac{7}{3}}} \\ &A = a\frac{z-d}{L} + b \,(\text{stable}) \\ &A = b \,(\text{unstable}) \\ &B = 0.75A^{-\frac{4}{3}} \\ &n = f(z-d)/U \end{aligned} \quad (2)$$

where $U$ is the average horizontal wind velocity, $z$ is the observation height, and $d$ is the zero plane displacement (15.9 m). The parameter $A$ was optimized for each 30-min observation of normalized co-spectral density values of $w$ and $t$. The present analysis used 10,144 datasets (30 April–31 December 2002). Parameters $a$ and $b$, which determine $A$, were 0.217 and 0.420, respectively, and were determined using the relationship between optimized $A$ and $(z-d)/L$. The normalized co-spectra of $wt$ in this model depend only on the measurement height and wind velocity under unstable and neutral conditions and also on stability under stable conditions. Observations match the model with the peak in co-spectra occurring at a higher frequency than in Kaimal and Finnigan (1994) or Moore (1986). The relationship between $A$ and stability matches the generalization of Kaimal and Finnigan (1994) based on Kaimal et al. (1972).

The transfer function TF($f$) is a simple approximation that uses a one-parameter sigma function as proposed by Aubinet et al. (2001):

$$TF(f) = \frac{\overline{w't'}}{\overline{w'h'}} \frac{C_{wh}(f)}{C_{wt}(f)} = \exp\left( -\ln(2)\frac{f^2}{f_0^2} \right), \quad (3)$$

where $f_0$ is the half-power frequency. The parameter $f_0$ and thus the shape of the transfer function depend on the observation system (Moore, 1986; Leuning and Moncrieff, 1990; Leuning and Judo, 1996). For a closed-path system, flux loss due to airflow down the tube is a matter of utmost concern. Leuning and Judo (1996), Moncrieff et al. (1997) and Massman (2000) developed theoretical model that estimates the transfer function of the system. The actual transfer function in field conditions had a lower half-power frequency as shown both by Aubinet et al. (2001) and in data used in this study. Furthermore, tube length, tube condition, and pumping flow rate changed after every maintenance session in our observation system. Thus, the entire path operation period (2 years) was divided into 44 observation periods. The optimal half-power frequency for each period was computed with observed co-spectral attenuation of the density fluctuation. The ratio of co-variances $\overline{w't'}/\overline{w'h'}$ was

$$\frac{\overline{w't'}}{\overline{w'h'}} = \frac{\int_{f_l}^{f_h} C_{wt}(f)\,df}{\int_{f_l}^{f_h} C_{wh}(f)\,df}, \quad (4)$$

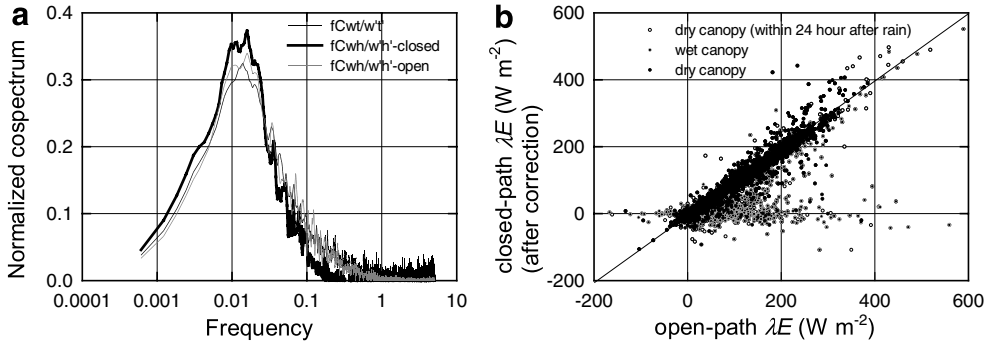



**Figure 3** Comparison of closed-path and open-path data. (a) An example of normalized cospectrum $fC_{wt}/w't'$, open-path $fC_{wh}/w'h'$, and closed-path $fC_{wh}/w'h'$, showing the high-frequency attenuation for the closed-path $fC_{wh}/w'h'$ case. The ensemble average that meets the conditions 1.0 m s$^{-1}$ < $U$ < 2.0 m s$^{-1}$, $R_n - S - G$ > 100 W m$^{-2}$, unstable, and $-0.4 < I < 0.2$ (calculated using closed-path $\lambda E$ before correction) from all available 30-min datasets between 21 May and 24 June 2002 was plotted ($n$ = 250). (b) The relationship between closed-path $\lambda E$ after high-frequency correction and open-path $\lambda E$. Black dots: dry canopy (all data from within 24 h after the end of rain were excluded). White dots: dry canopy within 24 h of rain. Gray dots: wet canopy (selection based on wetness sensor data). All available 30-min datasets that contained both closed-path and open-path $\lambda E$ between 30 April and 31 December 2002 were plotted ($n$ = 8103).

where $f_l$ and $f_h$ are the lowest and highest frequency limitations that allow an evaluation of the co-variance ratio unaffected by high frequency attenuation; $f_l$ and $f_h$ were set as 0.005 Hz and 0.01 Hz for most cases. The ensemble average of co-spectral density $C_{wt}(f)$ and $C_{wh}(f)$ of the dataset was used in the optimization procedure.

Fig. 3a shows an example (an ensemble average for one of the 44 observation periods) of normalized cospectrum $fC_{wt}/\overline{w't'}$, the open-path $fC_{wh}/\overline{w'h'}$, and the closed-path $fC_{wh}/\overline{w'h'}$. High-frequency attenuation is notable in the closed-path case. The ratio of corrected $\lambda E$ to original $\lambda E$ has a mean value of 1.15 after the attenuation correction. The ratio depends on the mean horizontal wind velocity, atmospheric stability, and the half-power frequency in the transfer function as determined from observed data. Closed-path $\lambda E$ matched open-path $\lambda E$ for the case of a dry canopy in a fine day after attenuation correction. However, the attenuation correction frequently underestimated open-path values regardless of canopy wetness (Fig. 3b) within 24 h of rain. Analysis of closed-path $\lambda E$ during and after rain (details in ''Energy budget closure'') requires care.

Sensible and latent heat fluxes observed in 2001, 2002, and 2003 were analyzed. The $\lambda E$ values discussed in the Results and Discussion sections refer to $\lambda E$ after frequency correction. Open-path data were used to analyze characteristics of evapotranspiration, closed-path data were used when open-path data were unavailable. In the compound dataset missing data comprised 33.9%, 14.1% and 3.7% of the total for $H$ in 2001, 2002, and 2003, and 38.5%, 20.0% and 9.9% of the total $\lambda E$ in 2001, 2002 and 2003, respectively. Missing data occurred because of quality control, system maintenance, sonic anemometer failure, IRGA failure, wiring failure, communication outages between the data logger and the computer, and power failures due to lightening and so on.

## Meteorological and energy balance measurements

Meteorological data were recorded using several data loggers (model CR10X, Campbell Scientific Inc., USA). The forest energy budget was estimated by

$$R_n = S\downarrow - S\uparrow + L\downarrow - L\uparrow = H + \lambda E + G + S + Q_p, \quad (5)$$

where $R_n$ is the net radiation, $S\downarrow$ and $S\uparrow$ are the downward and upward short-wave radiation, $L\downarrow$ and $L\uparrow$ are the downward and upward long-wave radiation, $G$ is the soil heat flux, $S$ is the change in total heat content of the forest air, water vapor, and biomass, and $Q_p$ is the energy of photosynthesis. The following imbalance expression shows the bias direction:

$$I = (H + \lambda E)/(R_n - G - S) - 1, \quad (6)$$

where $I$ is the imbalance ratio.

Downward and upward components of short-wave and long-wave radiation were measured at a height of 28.5 m with a four-component radiometer (model MR-40, EKO, Japan) until 27 December 2001 and by an albedo meter (CM14, Kipp & Zonen, Canada) and two long-wave radiometers (PIR, Eppley Laboratory, USA) after 27 December 2001. Soil heat flux was measured with heat flux plates (model MF81, EKO, Japan) installed at a depths of 0.01 m below the forest floor of the small catchment (see Fig. 1b) measured soil heat flux $G$. The forest canopy was closed. Spatial variability of $G$ was shown to be small by measurements using three heat flux plates mounted within a 10-m circle centered on the flux tower. One plate was between trunks, one was close to a trunk (*C. obtusa*) and one was just under a floor tree (*E. japonica*). The average absolute difference of the value of the sensor used in data processing from 2001 to 2003 from the average value of the three sensors was 2 W m$^{-2}$. The standard deviation was 2 W m$^{-2}$ for all data in 2004. Heat storage above 0.01 m was not computed.

Changes in total heat content of the forest air, water vapor, and biomass must be estimated so that energy closure can be evaluated (Wilson et al., 2002). Air temperature and relative humidity were measured by platinum thermometer and capacitive relative humidity (RH) sensor probes (model HMP45C, Vaisala, Finland) mounted in ventilated radiation shield cylinders at five heights (29, 20, 10, 4, and 1 m). These Vaisala sensors and thermocouples were periodically calibrated using an Assman psychrometer. Stem temperatures at heights of 1 m and 10 m and several depths were monitored using copper-constantan thermocouples for a stem (height: 18.5, diameter at breast height [DBH]: 20.8 cm) near the tower. Spatial variability of stem surface temperature was small based on measurements of four stems. The average absolute difference of the value of a stem used in data processing from 2001 to 2003 from the averaging value of the four stems was 0.13 °C; the standard deviation was 0.12 °C for all data between October 2003 and February 2004.

Heat storage terms were estimated as (Moore and Fisch, 1986)

$$S = Q_a + Q_w + Q_s, \quad (7)$$

where $Q_a$ and $Q_w$ are the change in heat storage forced by changes in canopy air temperature and specific humidity, respectively, and $Q_s$ is the change in heat storage associated with stem biomass. $Q_a$ and $Q_w$ can be written as

$$Q_a = \rho_a C_p \int_0^h \frac{dT_a}{dt} dz \quad (8)$$

$$Q_w = \rho_a \lambda \int_0^h \frac{dq_a}{dt} dz, \quad (9)$$

where $q_a$ is the specific humidity.

Census data and thermocouple measurements of stem surface temperatures were used to estimate the biomass heat storage $Q_s$. Analytical solutions of the heat-conduction equation for given diurnal cycles of the cylinder-surface temperature are described by Wada et al. (2002). Stem shape was approximated in the estimation procedure by a stack of 2-m-high cone-shaped cylinders. Biomass data were classified by their radii at each height. Estimates of heat conduction into a given stem (as a cylindrical material) were checked using thermocouple measurements of the temperature at several stem depths. When thermocouple surface temperatures were unavailable, air temperatures at 1 and 10 m were converted to a surface temperature using the same heat conduction equation and assuming an ''ideal cylinder'' with a surface temperature equal to the reference air temperature. This method was validated with observed results (Wada et al., 2002).

Soil water capillary pressure was measured at five depths (0.1, 0.2, 0.3, 0.5, and 1.0 m) below the soil surface using tensiometers at several points over the watershed. Reference soil water capillary pressure data were measured at the edge of a permanent water body in the small watershed where the flux tower was located. Energy of photosynthesis was neglected in this study. Fifteen handmade wetness sensors (Takanashi et al., 2003) mounted on leaves at five heights (between 15.3 and 11.3 m) measured canopy wetness to monitor canopy conditions (wet or dry) and estimate the transition time from evaporation to transpiration during and after rain.

### Parameterization of the bulk canopy characteristics

Surface conductance ($g_c$) and the decoupling factor ($\Omega$) were calculated using the Penman–Monteith equation (Monteith, 1973) and the expression by McNaughton and Jarvis (1983):

$$\lambda E = \frac{\Delta(R_n - G - S) + \rho C_p g_a (e_s(T_a) - e_a)}{\Delta + \gamma(1 + g_a/g_c)}, \quad (10)$$

$$\Omega = \left(\frac{\Delta/\gamma + 1}{\Delta/\gamma + 1 + g_a/g_c}\right), \quad (11)$$

where $\Delta$ is the slope of a function relating saturation vapor pressure to temperature (hPa $K^{-1}$), $\rho$ is air density (mol $m^{-3}$), $C_p$ is the specific heat capacity of air (J $mol^{-1}$ $K^{-1}$), $e_s(T_a)$ is saturation vapor pressure at air temperature (hPa), $e_a$ is vapor pressure of the air, $\gamma$ is the psychrometric constant (hPa $K^{-1}$), $g_a$ is aerodynamic conductance (m $s^{-1}$), and $g_c$ is surface (canopy) conductance (m $s^{-1}$). Aerodynamic conductance $g_a$ was calculated as

$$\frac{1}{g_a} = r_a = \frac{u_r}{u_*^2}, \quad (12)$$

where $r_a$ is the aerodynamic resistance, $u_r$ is the wind velocity at the reference height (m $s^{-1}$), and $u_*$ is the friction velocity (m $s^{-1}$). We did not count on the excess resistance for scalars in Eq. (12), mainly because the surface temperatures estimated by solving energy balance equation with any excess resistance would not agree with the estimated values from the upward long-wave radiation at 28.5 m. The equilibrium latent heat flux ($\lambda E_{eq}$) is defined as (Priestley and Taylor, 1972):

$$\lambda E_{eq} = \frac{\Delta(R_n - G - S)}{\Delta + \gamma} \quad (13)$$

## Results and discussion

### Energy budget closure

If evapotranspiration characteristics are to be evaluated with precision, the possibility of underestimating heat fluxes as measured with the eddy covariance method must be checked. The energy balance closure was assessed to validate sensible and latent heat flux as measured by the eddy covariance both with closed path and open path systems. Fig. 4 shows sensible + latent heat flux versus available energy for open-path system data ($n$ = 10,453) and closed-path system data ($n$ = 11,107) for 2002. The data are divided into two categories based on canopy wetness as measured by the wetness sensors. Fig. 4 also lists regression coefficients. The slopes of open-path and closed-path linear regressions forced through the origin were 0.90 and 0.87 for the dry-canopy and 0.93 and 0.72 for the wet-canopy. Fig. 4 also shows a significant lack of energy balance for closed path system measurements during and after rain. Energy imbalances at the site for other cases resembled values at other forest sites (Wilson et al., 2002; Turnipseed et al., 2002).

Fig. 5 shows $\lambda E$ values from eddy covariance (both open- and closed-path systems) and the residual of energy balance equation (=$R_n - G - S - H$) during and after rain, along with canopy wetness and precipitation for 3 days (9–11 November 2002). The closed-path $\lambda E$ did not detect evaporation during and after rain because of notable high frequency attenuation of $fC_{wh}/\overline{w'h'}$. For example, the half-power frequency $f_0$ of the transfer function used in the frequency correction for the period shown in Fig. 5 was 0.087. This value shifted to around 0.02 during and after rain (as detected from the average $fC_{wh}/\overline{w'h'}$ and $fC_{wt}/\overline{w't'}$ from 9:00 to 14:00 on 9 November 2002). Most of the co-spectra that

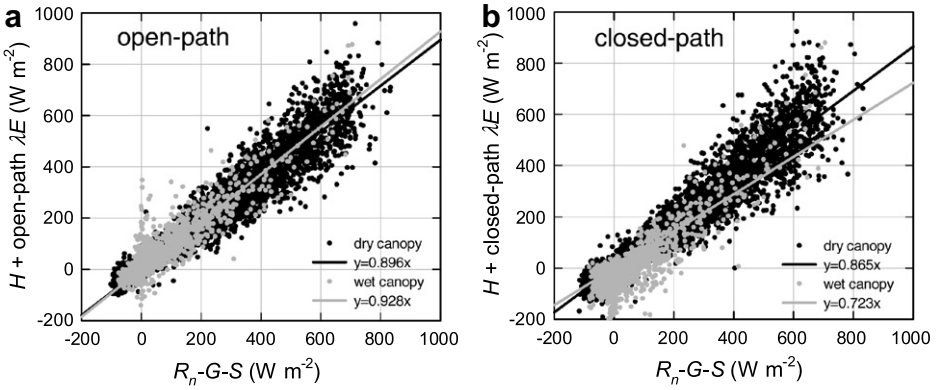



**Figure 4** Plots of $H + \lambda E$ ((a): open-path; (b): closed path) versus available energy ($R_n - G - S$). Black dots show dry canopy data, and gray dots show wet canopy data. Wetness was determined from wetness sensor data. All available 30-min datasets including all components of the energy budget in 2002 ($n$ = 11,107 for closed-path data, and $n$ = 10,453 for open-path data) were plotted.

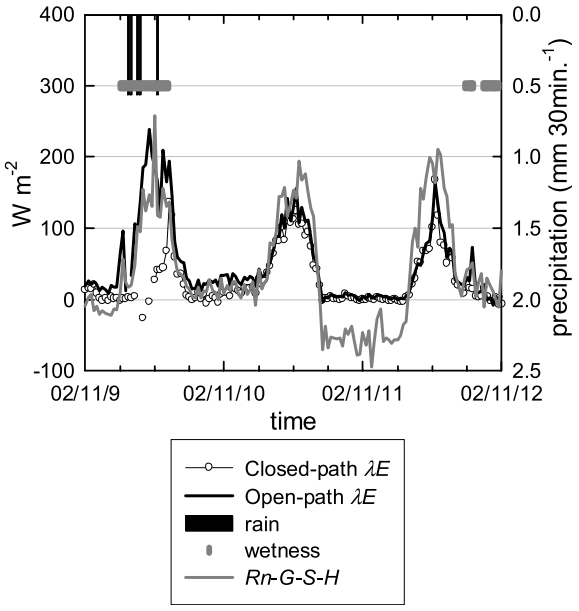



**Figure 5** $\lambda E$ values from eddy covariance (both open- and closed-path systems) and the residual of energy balance equation ($=R_n - G - S - H$) during and after rain, along with canopy wetness and precipitation for 3 days (9—11 November 2002).

form the latent heat flux were therefore lost through high frequency attenuation. This phenomenon mostly corrected itself on the following day (also see Fig. 3b). In contrast, open-path $\lambda E$ satisfactorily detected evapotranspiration during and after rain, except for an occasional spike (data not shown) during rainfall when raindrops lingered on the lens of the LI7500 sensor. Comparison of closed-path and open-path data revealed that closed-path calculations yielded underestimates during and after precipitation, and consequently resulted in considerable underestimation of the evapotranspiration.

Fig. 6 shows diurnal changes of each energy budget component and the total imbalance ratio. The average diurnal changes for the storage terms ($Q_s$, $Q_a$, $Q_w$, and $G$) and their total in ratio to $R_n$ for all days in 2002 are shown in Fig. 6a. Fig. 6b shows the average diurnal changes of $R_n$, $H$, $\lambda E$, and the imbalance ratio from averaging all available data in 2002, except for 24 h after rain. Open-path data were used for averaging; where open path data were unavailable, closed-path data were used. Storage terms were 20—30% of $R_n$ at night, 5—60% in the morning, and 2—5% in the afternoon. The largest component of the nocturnal heat storage terms was negative heat storage by biomass. Changes in total heat content of the forest air and water vapor are not negligible in the energy budget. The energy budget improved in the morning and at night when these components were considered (see Fig. 6b). The aggregate imbalance ratio $I$ was about −0.1 (90% closure) during the day and −0.5 (50% closure) at night. Analysis of the co-spectra of the site showed that the potential loss of low frequency contribution was 1—2% when the averaging time was 30 min compared to the case with an averaging time of 60 min. Other possibilities should be considered as a cause of the imbalance.

Fig. 7a and b shows the imbalance ratio versus friction velocity $u_*$ during night and day, respectively. Data were classified for every 0.1 m s$^{-1}$ of $u_*$; average values and standard error for each class are shown by a dot and error bar on the top of each figure. Standard deviations for each class are shown by bar graphs in the middle of each figure. The standard deviation of $I$ in this analysis represents the temporal variability of $I$ and relates to spatial variability of $I$ for flux data measured at a tower if the sampling numbers are sufficient. Bar graphs at the bottom of the figure show frequency. Data were segregated into three wind directions. At the study site, the predominant daytime wind directions were mainly northerly and sometimes westerly regardless of season. The imbalance ratio approaches zero as turbulent intensity ($u_*$) increases, probably because advection effects decrease. Other researchers have reported similar results (e.g., Turnipseed et al., 2002; Wilson et al., 2002). The decrease in the standard deviation of $I$ as $u_*$ increases suggests an improvement in the spatial representativeness of the data. Fig. 7b suggests $I$ was nearly zero during the day when

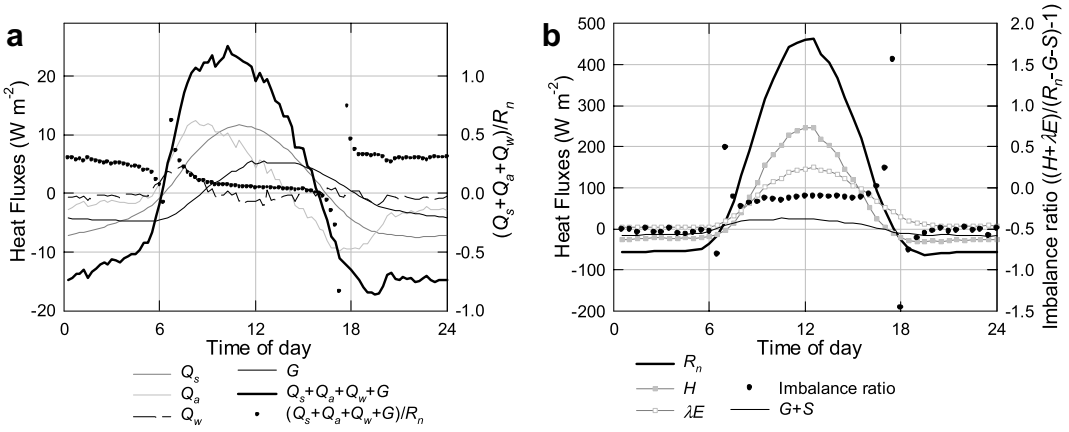



**Figure 6** Diurnal changes of each component in the energy budget for the total imbalance ratio. (a) The average diurnal change in storage terms ($Q_s$, $Q_a$, $Q_w$, $G$) and their total in ratio to $R_n$ for all days in 2002. (b) Average diurnal changes in $R_n$, $H$, $\lambda E$, $G + S$ and imbalance ratio for each day in 2002, except for the data within 24 h of rain. Open-path data were used for averaging; closed-path data were substituted when open-path data were unavailable.

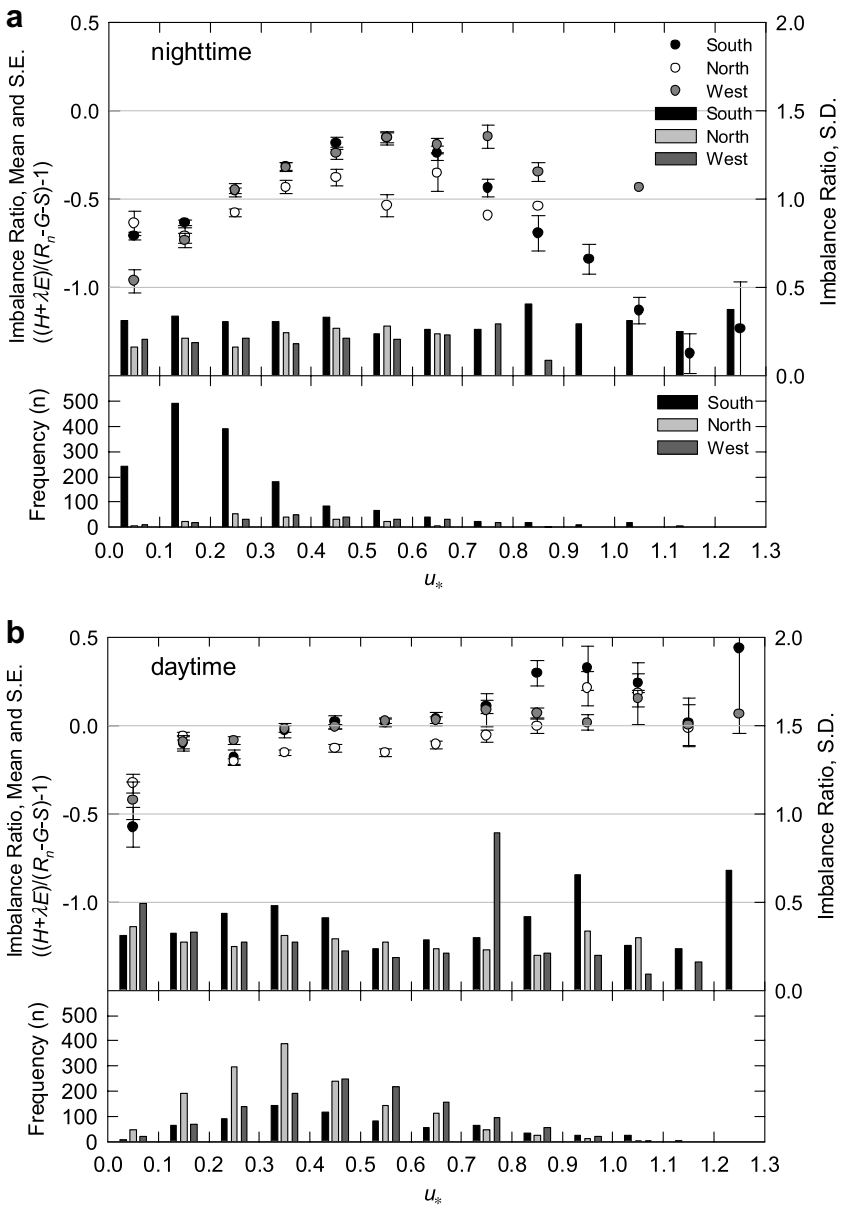



**Figure 7** Imbalance ratio versus friction velocity $u_*$ during (a) night and (b) day. Data were classified into every 0.1 m s$^{-1}$ of $u_*$; average values with a standard error for each class are shown by dots and error bars in each figure. Standard deviations for each class are shown as bar graphs. Frequencies are shown as bar graphs at the bottom of the diagram. Data were segregated for three major wind directions. Open-path $\lambda E$ values were used in this analysis, and all available 30-min datasets from 30 April to 31 December 2002 that contained all components were used ($n$ = 5478). Points with $\overline{u'w'} > 0$ are excluded in this figure, as $u_*$ cannot be calculated from positive $\overline{u'w'}$; however, such points were not omitted from other analyses in the paper.

the friction velocity was large. Closer inspection, however, shows negative $I$ even for large friction velocities, especially for northerly winds, which occurred with the highest frequency during the day. The average $I$ was about −0.1 during the day as shown in Fig. 6b; a regression analysis of $H + \lambda E$ versus available energy yielded a slope of 0.90–0.93. A more distinct relationship between $u_*$ and $I$ existed at night, and $I$ for a high turbulent intensity was approximately −0.2. The larger negative imbalance at night suggests nocturnal terrain-induced drainage flow. Imbalances increase at night for large $u_*$, perhaps because small high-frequency fluctuations of temperature were obscured by noise in the sonic anemometer, as demonstrated by Turnipseed et al. (2002). The standard deviation of $I$ was larger for south winds than for other wind directions, reflecting terrain complexity and associated horizontal heterogeneity in that direction. Increased variability occurred because the edge of the small watershed was south of the tower. Analysis of integral turbulence characteristics (Aubinet et al., 2000) also showed larger deviation from the expected line in the case of south wind, which suggests the lack of horizontal homogeneity.

Imbalances, especially for cases with southerly winds, rain, or large $u_*$ at night, are caused by technical difficulties

or topographical effects associated with the complex terrain. Energy imbalances in other cases may also be caused by the sum of the various small errors. The error related with the sonic anemometer structure is one of the possible sources of flux undermeasurement (e.g., Gash and Dolman, 2003; van der Molen et al., 2004). However, imbalances may also suggest the presence of mean vertical advection as noted in a large eddy simulation (LES) study by Watanabe and Kanda (2002). This LES study showed that eddy covariance systematically underestimates fluxes if fluxes due to stationary eddies make a large contribution to the total area-averaged fluxes. In our study, daytime latent heat flux from a dry canopy for wind directions other than south could be estimated from good quality data in this forest, despite problems introduced by complex terrain. The sensible and latent heat fluxes were adjusted using the Bowen ratio to impose energy balance closure during the day. Any residuals were attributed to the sensible heat flux at night. If not all components of the energy budget were available, the fluxes were corrected by dividing by a constant (Kumagai et al., 2004). The values for this constant were taken as 0.9 during daytime and 1.0 at night. Open-path data after correction were basically used for the analysis, and closed-path data after correction were used when open-path data were unavailable. The latent heat flux during and after rain (within 24 h of the end of the rain) in the closed-path data was replaced in the eddy correlation/energy balance $\lambda E$ ($=R_n - G - S - H$), using $H$ after corrections, where $R_n$ is the net radiation, $G$ the soil heat flux, and $S$ the change in the total heat content of the forest air, water vapor, and biomass. Gaps were also filled using the energy balance equation if data for only one of $\lambda E$ of $H$ were missing. After this procedure, the coverage of data became 68.4%, 87.6% and 96.2% of the total for $\lambda E$ in 2001, 2002, and 2003, respectively.

## Characteristics of sensible and latent heat fluxes — annual and seasonal variability

Characteristics of sensible and latent heat fluxes in the Japanese cypress forest were analyzed using the compound dataset after corrections. This forest is an example of a temperate evergreen coniferous forest, and data were analyzed for inter-annual and seasonal variability. Daily values including the midday average were provided only if more than 90% of the data on that day were available for each component. Such data were mostly free from the gap-filling influences. Annual records of evapotranspiration were calculated with two gap filling methods as mentioned below. This procedure could cause a negligible error in the annual total evapotranspiration for 2001, when 31.6% of the data were missing.

Fig. 8 shows daily aggregate solar radiation, net radiation, air temperature, and vapor pressure deficit (VPD) at 20-m heights as well as precipitation and soil water capillary pressure. Precipitation total were 1438, 1179, and 1971 mm in 2001, 2002 and 2003, respectively. The 33-year average (1972—2004) of annual precipitation was 1645 mm; 2002 was the second-driest year on record, after 1030 mm in 1994. Soil capillary pressure at the surface in late summer of which year reached −500 cm. However, even in the driest year, underground water and stream runoff from the whole watershed (5.99 ha) persisted. In contrast, 2003 was one of the wettest years, with 1971 mm of rain. Daily average air temperature ranged between 0 and 30 °C. Daily solar radiation was largest in May;

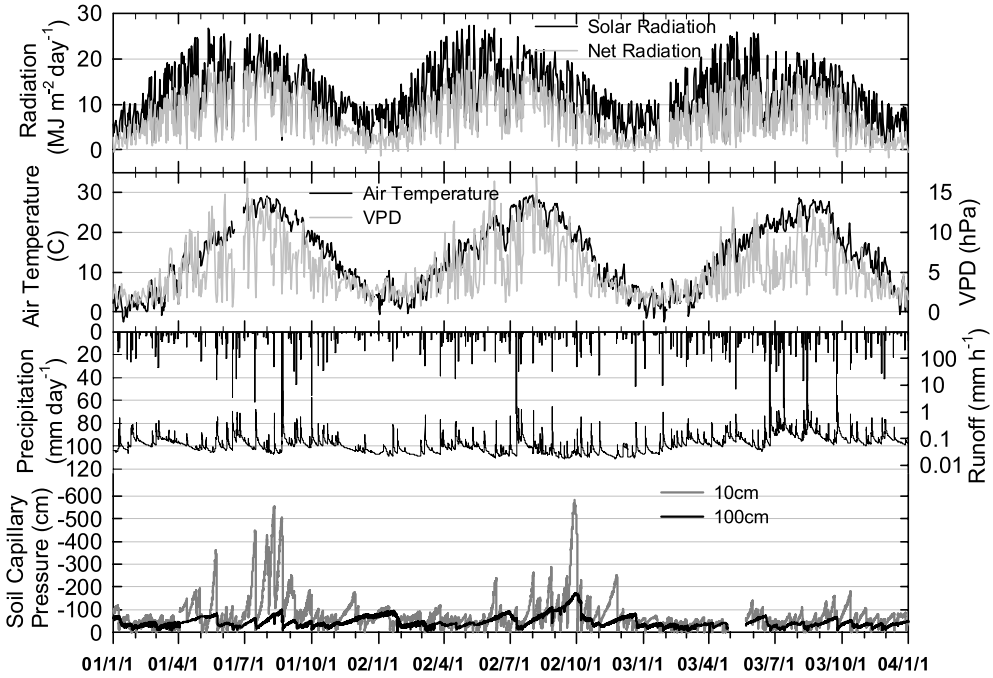



**Figure 8** Daily aggregate surface precipitation and solar radiation, net radiation, air temperature, and VPD at height of 20 m, and soil water capillary pressure at the edge of the permanent water body in the small watershed where the flux tower was located.

**Table 1** Summary of climatology, evapotranspiration, and bulk canopy characteristics

| Variable | 2001 | 2002 | 2003 | Average |
|---|---|---|---|---|
| Precipitation (mm) | 1438 | 1179 | 1971 | 1529 |
| Temperature (°C) | 13.2 | 13.4 | 12.9 | 13.2 |
| Solar radiation (GJ $m^{-2}$) | 4.45 | 4.57 | 4.04 | 4.35 |
| Net radiation (GJ $m^{-2}$) | 2.91 | 2.70 | 2.43 | 2.68 |
| Evapotranspiration(1) (mm) | 720 | 735 | 750 | 735 |
| % Flux data coverage(1) | 68.4 | 87.6 | 96.2 | 84.0 |
| Evapotranspiration(2)(mm) | 710 | 735 | 742 | 729 |
| Days of flux data coverage(2) | 205 | 289 | 336 | 277 |
| Equilibrium evaporation $\lambda E_{eq}$ (mm) | 813 | 769 | 686 | 756 |
| Bowen ratio, midday dry canopy (midseason) | 1.08 | 1.18 | 1.05 | 1.10 |
| $g_c$, midday dry canopy (midseason) (mm $s^{-1}$) | 6.8 | 6.3 | 7.0 | 6.7 |
| $\Omega$, midday dry canopy (midseason) | 0.22 | 0.19 | 0.22 | 0.21 |
| $\alpha$, midday dry canopy (midseason) | 0.67 | 0.66 | 0.78 | 0.70 |

The annual mean air temperature measured at an open screen site was used here as a reference value for the site. Calculations of the annual evapotranspiration were (1) based on corrected 30-min fluxes and gaps were filled with the annual average value, or (2) based on daily values which were provided only if more than 90% data on that day was available and gaps were filled with the relationships between daily latent heat flux and daily average vapor pressure deficit for three cases of rainy days, the days following rainy days, and fair days. Bulk parameters were calculated by averaging every available daily value. Midseason refers to June–October. Midday averages for each day were calculated by averaging all available 30-min data (>90%) between 10:00 and 15:00. Bowen ratio was calculated using averaged values of $H$ and $\lambda E$ during midday. Days with rain and the following day were omitted to avoid wet canopy data.

and often small in June and early July because of rains associated with the ''Baiu'' front. Rainy conditions in 2003 reduced the incoming radiation through the summer season. Consequently, 2003 had less solar radiation than 2001 or 2002 (Table 1, Fig. 8).

The annual amount of evapotranspiration was estimated to be 720 mm (2001), 735 mm (2002) and 750 mm (2003) if calculation was made using every available 30-min dataset and gaps were filled with the annual average value, or estimated to be 710 mm (2001), 735 mm (2002) and 742 mm (2003) if calculation was made using daily values which were provided only if more than 90% of the data on that day was available and gaps were filled with the relationships between daily latent heat flux and daily average vapor pressure deficit for three cases; i.e., rainy days, days following rainy days and fine days (see Fig. 9d–f). Average annual evapotranspiration was 735 mm with former estimation. These values were similar to the Priestley–Taylor equilibrium evaporation (756 mm for 3-year average) with a little fluctuation (89–109%). Evapotranspiration at the study site exceeded that for a broadleaf temperate deciduous forest (567 mm) with similar climatology (precipitation: 1454 mm, temperature: 14.9 °C, equilibrium evapotranspiration: 835 mm; Wilson and Baldocchi, 2000). Inter-annual fluctuations in evapotranspiration between dry (2001, 2002) and wet (2003) years were not distinct (Table 1). Relationships between daily latent heat flux and VPD in the dry canopy (Fig. 9d) in each year also showed no significant differences between wet and dry years. The relationship reaches the upper limit at large VPD, so a little smaller VPD in wet year seemed to have little effects on the amount of evapotranspiration.

Fig. 9a–c shows the seasonal changes in the daily amount of sensible heat flux, latent heat flux, and $\alpha$ ($\lambda E/\lambda E_{eq}$), respectively. Data for days with or following rain were distinguished with white dots in this figure to make clear the dry canopy characteristics. In the case of dry canopy, maximum latent heat flux occurred in summer and early autumn. Seasonal changes in latent heat flux in a dry canopy roughly track seasonal changes in vapor pressure deficit (Fig. 9d); sensible heat flux thus balanced the radiation budget with a maximum in early spring. The actual dry canopy transpiration was less than the Priestley–Taylor $\lambda E_{eq}$ especially at large VPD (Fig. 9c and d), which suggests a physiological regulation. In late autumn (from mid-October to December), $\alpha$ sometimes became quite large and made no sense because of the small daily base net radiation. Fig. 10a–c shows midday values (average of calculated values using 30-min meteorological and flux data from 10:00 to 15:00) of the Bowen ratio, surface conductance and $\Omega$ respectively, for the dry canopy. The Bowen ratio was calculated using average values of $H$ and $\lambda E$ during midday (10:00–15:00). Data from days with or following rain were omitted from this figure. The midday average dry canopy Bowen ratio was 1.08 (2001), 1.18 (2002), and 1.05 (2003) during midseason (June–October) and increased in winter. The midday average dry canopy surface conductance was 6.8 (2001), 6.3 (2002), and 7.0 (2003) during midseason and decreased in winter. The midday average dry canopy $\Omega$ was 0.22 (2001), 0.19 (2002), and 0.22 (2003) during midseason and decreased in winter. The midday average dry canopy $\alpha$ was 0.67 (2001), 0.66 (2002) and 0.78 (2003) during midseason (Table 1). Our study site was characterized by small values of surface conductance and decoupling factor compared to other forests. However, the values are slightly larger than values in several other coniferous forests (Baldocchi et al., 1997; Kelliher et al., 1997, 1998; Humphreys et al., 2003); surface conductance plays an important role in regulating dry canopy transpiration. Inter-annual

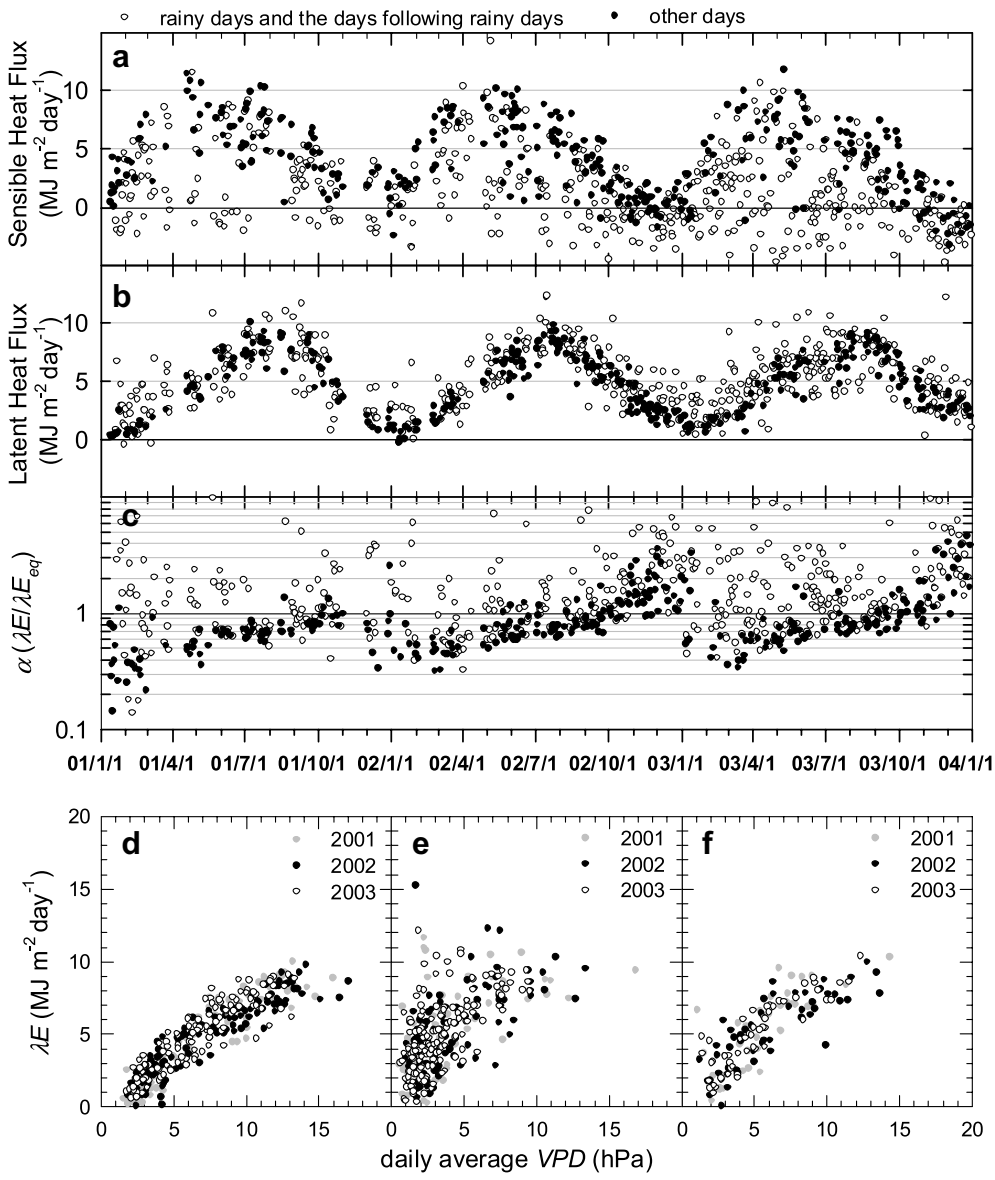



**Figure 9** Seasonal variations in the daily (a) sensible heat flux, (b) latent heat flux, and (c) Priestley—Taylor $\alpha$ coefficient in 2001, 2002, and 2003, and the relationships between daily latent heat flux and daily mean VPD on (d) fair days, (e) rainy days, and (f) days following rainy days. The $\alpha$ coefficient in (c) was calculated from the daily amount of $\lambda E$ and $\lambda E_{eq}$. Black and white dots in (a)—(c) represent fair days, and days with rain and the following day; Gray, black and white dots in (d)—(f) represent 2001, 2002, and 2003, respectively.

fluctuations in bulk parameters were relatively small, although surface conductance and the corresponding $\alpha$ were slightly larger in wet years. Differences were mitigated by differences in dry canopy latent heat flux because of smaller VPD in wet years (Fig. 9d).

Fig. 11 shows the relationship between midday average $g_c$ and midday average VPD in each year. No significant difference in $g_c$ — VPD was observed between wet and dry years; soil droughts did not affect the bulk surface conductance at this site for these years. This is in contrast to results for a forest of a Douglas-fir forest (Humphreys et al., 2003), a different type of evergreen coniferous forests, that did show differences in $g_c$ — VPD related to soil moisture conditions for similar annual precipitation as our site. The difference may be related to differences in the strength of the summer soil drought; the site studied by Humphreys et al. (2003) received most precipitation in winter. Surface conductance in winter was small regardless of VPD and also solar radiation. This suggests a phenological constraint. Japanese cypress trees experience leaf growth continuously from late April to October. Some old leaves fall in late autumn. In winter (from January to March), some of the canopy leaves in Japanese cypress forests turn reddish. The red pigment prevents the light inhibition. Small surface conductance in winter may be influenced by this phenological cycle. Stomatal conductance on canopy leaves also became quite small in winter (unpublished data).

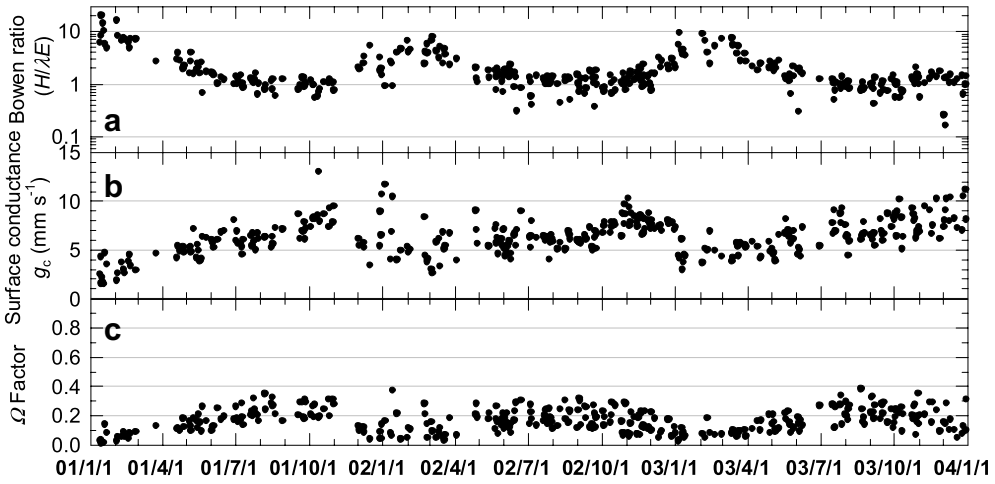



**Figure 10** Seasonal changes in midday Bowen ratio, surface conductance, and the decoupling factor calculated by averaging values from 10:00 to 15:00 using 30-min meteorological and flux datasets (=midday average). The Bowen ratio was calculated using average values of $H$ and $\lambda E$ during midday. Data on days with or following rain were omitted from this figure.

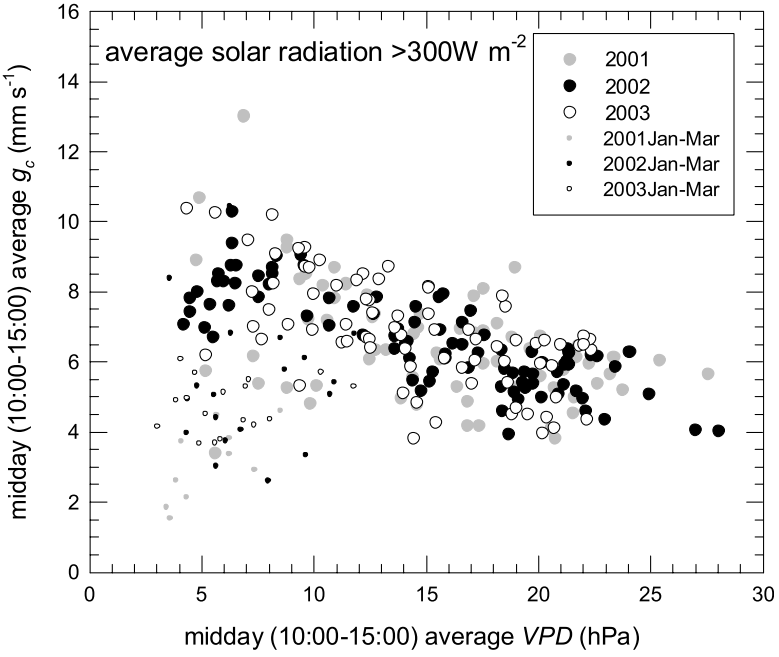



**Figure 11** Relationship between midday average surface conductance and midday average VPD in dry years (2001, 2002) and a wet year (2003). Only data from days when the average midday solar radiation exceeded 300 W/m$^2$ were considered. Data for rainy days and days following rainy days were excluded. Gray, black and white dots in (d)—(f) represent 2001, 2002, and 2003, respectively. Smaller dots represent data between January and March for each year.

## Conclusions

Three years of continuous eddy covariance measurements of sensible and latent heat flux above a Japanese Cypress forest with complex topography yielded information on the magnitude and seasonal and inter-annual variations in sensible and latent heat fluxes, evapotranspiration, and parameters representing the bulk canopy characteristics. This cypress forest was an example of temperate evergreen coniferous forest. Average annual evapotranspiration for 3 years was 735 mm. Inter-annual fluctuations in evapotranspiration were small despite large precipitation fluctuations over the 3 years.

This Japanese cypress forest study site showed some of the smallest values of surface conductance and decoupling factor among various forest types. However, these values were slightly larger than those of several other coniferous forests in cooler climate regions. Surface conductance and stomatal regulation plays an important role in regulating dry-canopy transpiration in this forest. However, the inter-annual fluctuations in bulk parameters were relatively small and variations in surface conductance characteristics

affected by soil moisture conditions were not observed between dry and wet years.

## Acknowledgements

The authors thank the pioneers and current colleagues who with us have struggled with eddy covariance flux observations at this site. The research was initiated by Dr. Masakazu Suzuki in 1990, pioneered by Mr. Akihiro Nakamura, Dr. Katsunori Tanaka, Dr. Motomu Toda, and Mr. Katsuaki Tachibana. The framework for frequency correction and the base program for spectral analysis were provided by Mr. Katsuaki Tachibana. Meteorological observations from 2002 to 2003 was conducted with Mr. Tomonori Mitani. We thank Dr. Nobutaka Monji and Dr. Ken Hamotani, who provided the radiation data during missing periods, Dr. Masanori Katsuyama, who provided rain and runoff data and the site contour map, and Dr. Masatoshi Kawasaki and Mr. Kenichi Osaka, who provided soil water capillary pressure data.

This work was supported by the Global Environment Research Fund of the Japan Environment Agency, and by grants for scientific research from the Ministry of Education, Culture, Sports, Science, and Technology, Japan.

## References

Aubinet, M., Grelle, A., Ibrom, A., Rannik, U., Moncrieff, J., Foken, T., Kowalski, A.S., Martin, P.H., Berbigier, P., Bernhofer, Ch., Clement, R., Elbers, J., Granier, A., Grunwald, T., Morgenstern, K., Pilegaard, K., Rebmann, C., Snijders, W., Valentini, R., Vesala, T., 2000. Estimates of the annual net carbon and water exchange of forests: the EUROFLUX methodology. Adv. Ecol. Res. 30, 113–175.

Aubinet, M., Chermanne, B., Vandenhaute, M., Longdoz, B., Yernaux, M., Laitat, E., 2001. Long term carbon dioxide exchange above a mixed forest in the Belgian Ardennes. Agric. For. Meteorol. 108, 293–315.

Baldocchi, D.D., Vogel, C.A., Hall, B., 1997. Seasonal variation of energy and water vapor exchange rates above and below a boreal jack pine forest canopy. J. Geophys. Res. 102, 28939–28951.

Blanken, P.D., Black, T.A., Yang, P.G., Neuman, H.H., Nesic, Z., Staebler, R., den Hartog, G., Novak, M.D., Lee, X., 1997. Energy balance and surface conductance of a boreal aspen forest: Partitioning overstory and understory components. J. Geophys. Res. 102 (D24), 28915–28927.

Culf, A.D., Foken, T., Gash, J.H.C., 2004. The energy balance closure problem. In: Kabat, P., Claussen, M., Dirmeyer, P.A., Gash, J.H.C., Bravo de Guenni, L., Meybeck, M., Pielke, R.S., Vörösmarty, C.J., Hutjes, R.W.A., Lütkemeier, S. (Eds.), Vegetation, Water, Humans and the Climate. Springer-Verlag, Berlin, pp. 159–166.

Foken, T., Wichura, B., 1996. Tools for quality assessment of surface-based flux measurements. Agric. For. Meteorol. 78, 83–105.

Fukushima, Y., 1988. A model of river flow forecasting for a small forested mountain catchment. Hydrol. Process. 2, 167–185.

Gash, J.H.C., Dolman, A.J., 2003. Sonic anemometer (co)sine response and flux measurement. I. The potential for (co)sine error to affect sonic anemometer-based flux measurements. Agric. For. Meteorol. 119, 195–207.

Grace, J., Lloyd, J., Mcintyre, J., Miranda, A., Meir, P., Miranda, H., Moncrieff, J., Massheder, J., Wright, I., Gash, J., 1995. Fluxes of carbon dioxide and water vapour over an undisturbed tropical forest in south-west Amazonia. Global Change Biol. 1, 1–12.

Hobara, S., Tokuchi, N., Ohte, N., Nakanishi, A., Katsuyama, M., Koba, K., 2001. Mechanism of nitrate loss from a forested catchment following a small-scale, natural disturbance. Can. J. For. Res. 31, 1326–1335.

Humphreys, E.R., Black, T.A., Ethier, G.J., Drewitt, G.B., Spittlehouse, D.L., Jork, E.-M., Nesic, Z., Livingston, N.J., 2003. Annual and seasonal variability of sensible and latent heat fluxes above a coastal Dauglas-fir forest, British Columbia, Canada. Agric. For. Meteorol. 115, 109–125.

Kaimal, J.C., 1988. The atmospheric boundary layer — its structure and measurement. Indian Institute of Tropical Meteorology, Pune.

Kaimal, J.C., Finnigan, J.J., 1994. Atmospheric Boundary Layer Flows: Their Structure and Measurement. Oxford University Press, Oxford.

Kaimal, J.C., Wyngaad, J.C., Izumi, Y., Cote, O.R., 1972. Spectral characteristics of surface layer turbulence. Q. J. R. Meteorol. Soc. 98, 563–589.

Kelliher, F.M., Leuning, R., Raupach, M.R., Schulze, E.-D., 1995. Maximum conductances for evaporation from global vegetation types. Agric. For. Meteorol. 73, 1–16.

Kelliher, F.M., Hollinger, D.Y., Schulze, E.-D., Vygodskaya, N.N., Byers, J.N., Hunt, J.E., McSeveny, T.M., Milukova, I., Sogatchev, A., Verlargin, A., Ziegler, W., Arneth, A., Bauer, G., 1997. Evaporation from an eastern Siberian larch forest. Agric. For. Meteorol. 85, 135–147.

Kelliher, F.M., Lloyd, J., Arneth, A., Byers, J.N., Mcseveny, T.M., Milukova, I., Grigoriev, S., Panfyorov, M., Sogatchev, A., Verlargin, A., Ziegler, W., Bauer, G., Schulze, E.-D., 1998. Evaporation from a central Siberian pine forest. J. Hydrol. 205, 279–296.

Komatsu, H., 2003. Relationship between canopy height and the reference value of surface conductance for closed coniferous stands. Hydrol. Process. 17, 2503–2512.

Kondo, J., Sato, T., 1982. The determination of the von Karman Constant. J. Meteorl. Soc. Jpn. 60, 461–474.

Kumagai, T., Saitoh, T., Sato, Y., Morooka, T., Manfroi, O., Kuraji, K., Suzuki, M., 2004. Transpiration, canopy conductance and the decoupling coefficient of a lowland mixed dipterocarp forest in Sarawak, Borneo: dry spell effects. J. Hydrol. 287, 237–251.

Lee, X., 1998. On micrometeorological observations of surface-air exchange over tall vegetation. Agric. For. Meteorol. 91, 39–49.

Leuning, R., Judo, M.J., 1996. The relative merits of open- and closed-path analysers for measurement of eddy fluxes. Global Change Biol. 2, 241–253.

Leuning, R., Moncrieff, J., 1990. Eddy-covariance $CO_2$ flux measurements using open- and closed path $CO_2$ analyzers: corrections for analyzer water vapor sensitivity and damping of fluctuations in air sampling tubes. Bound. Lay. Meteorol. 53, 63–76.

Mahrt, L., Vickers, D., Howell, J., Hojestrup, J., Wilczak, J.M., Deson, J., Hare, J., 1996. Sea surface drag coefficients in the Riso Air sea experiment. J. Geophys. Res. 101, 14327–14335.

Massman, W.J., 2000. A simple method for estimating frequency response corrections for eddy covariance systems. Agric. For. Meteorol. 104, 185–198.

Mcmillen, R.T., 1988. An eddy correlation technique with extended applicability to non-simple terran. Bound. Lay. Meteorol. 43, 231–245.

McNaughton, K.G., Jarvis, P.G., 1983. Predicting effects of vegetation changes on transpiration and evaporation. In: Kozlowski, T.T. (Ed.), Water Deficit and Plant Growth, vol. 7. Academic Press, New York, pp. 1–47.

Moncrieff, J.B., Massheder, J.M., de Bruin, H., Elbers, J., Friborg, T., Heusinkveld, B., Kabat, P., Scott, S., Soegaad, H., Verhoef, A., 1997. A system to measure surface fluxes of momentum, sensible heat, water vapor and carbon dioxide. J. Hydrol. 188—189, 589—611.

Monteith, J.L., 1973. Principles of Environmental Physics. Edward Arnold, London, 241 pp.

Moore, C.J., 1986. Frequency response corrections for eddy correlation systems. Bound. Lay. Meteorol. 37, 17—35.

Moore, C.J., Fisch, G., 1986. Estimating heat storage in Amazonian tropical forest. Agric. For. Meteorol. 38, 147—169.

Ohte, N., Tokuchi, N., Suzuki, M., 1995. Biogeochemical influences on the determination of water chemistry in a temperate forest basin: factors determining the pH value. Water Resour. Res. 31, 2823—2834.

Ohte, N., Tokuchi, N., Suzuki, M., 1997. An in situ lysimeter experiment on soil moisture influence on inorganic nitrogen discharge from forest soil. J. Hydrol. 195, 78—98.

Priestley, C.H.B., Taylor, R.J., 1972. On the assessment of surface heat flux and evaporation using large-scale parameters. Mon. Weather Rev. 100, 81—92.

Roberts, J.M., Gash, J.H.C., Tani, M., Bruijnzeel, L.A., 2005. Controls of evaporation in lowland tropical rainforest. In: Bonell, M., Bruijnzeel, L.A. (Eds.), Forests, Water and People in the Humid Tropics. Cambridge University Press, pp. 287—313.

Schuepp, P.H., Leclerc, M.Y., MacPherson, J.I., Desjardins, R.L., 1990. Footprint prediction of scalar fluxes from analytical solutions of the diffusion equation. Bound. Lay. Meteorol. 50, 335—373.

Takanashi, S., Kosugi, Y., Tani, M., Ohte, N., Yano, M., Tanaka, H., Tanaka, K., 2003. Evaporatranspiration from a Japanese cypress forest during and after rainfall. J. Jpn. Soc. Hydrol. Water Resour. 16, 268—283 (in Japanese with English abstract).

Takanashi, S., Kosugi, Y., Tanaka, Y., Yano, M., Katayama, T., Tanaka, H., Tani, M., 2005. $CO_2$ exchange in a temperate Japanese cypress forest compared with that in a cool-temperate deciduous broad-leaved forest. Ecol. Res. 20, 313—324.

Tani, M., Nik, A.R., Ohtani, Y., Yasuda, Y., Sahat, M.Md., Kasran, B., Takanashi, S., Noguchi, S., Yusop, Z., Watanabe, T., 2003. Characteristics of energy exchange and surface conductance of a tropical rain forest in Peninsular Malaysia. In: Ecology of a Lowland Rain Forest in Southeast Asia. Springer-Verlag, Tokyo, p. 628.

Turnipseed, A.A., Blanken, P.D., Anderson, D.E., Monson, R.K., 2002. Energy budget above a high-elevation subalpine forest in complex topography. Agric. For. Meteorol. 110, 177—201.

van der Molen, M.K., Gash, J.H.C., Elbers, J.A., 2004. Sonic anemometer (co)sine response and flux measurement. II. The effect of introducing an angle of attack dependent calibration. Agric. For. Meteorol. 122, 95—109.

Wada, T., Tani, M., Kosugi, Y., Takanashi, S., 2002. Estimation of biomass heat storage in a Hinoki (*Chamaecyparis obtusa*) forest. Forest Reserch, Kyoto 74, 69—76 (in Japanese with English abstract).

Watanabe, T., Kanda, M., 2002. LES study on the energy imbalance problem with eddy covariance fluxes. II: Analysis for a neutrally stratified surface boundary layer above and within a homogeneous plant canopy. J. Jpn. Soc. Hydrol. Water Resour. 15, 253—263.

Webb, E.K., Pearman, G.I., Leuning, R., 1980. Correction of flux measurements for density effects due to heat and water vapour transfer. Q. J. R. Meteorol. 106, 85—100.

Wilczak, J.M., Oncley, S.P., Stage, S.A., 2001. Sonic anemometer tilt correction algorithms. Bound. Lay. Meteorol. 99, 127—150.

Wilson, K.B., Baldocchi, D.D., 2000. Seasonal and interannual variability of energy fluxes over a broadleaved temperate deciduous forest in North America. Agric. For. Meteorol. 100, 1—18.

Wilson, K.B., Goldstein, A., Falge, E., Aubinet, M., Baldocchi, D., Berbigier, P., Bernhofer, C., Ceulemans, R., Dolman, H., Field, C., Grelle, A., Ibrom, A., Law, B.E., Kowalski, A., Meyers, T., Moncrieff, J., Monson, R., Oechel, W., Tenhunen, J., Valentini, R., Verma, S., 2002. Energy balance closure at FLUXNET sites. Agric. For. Meteorol. 113, 223—243.